Biomaterials 220 (2019) 119396

Contents lists available at ScienceDirect

Biomaterials

journal homepage: www.elsevier.com/locate/biomaterials

A three-dimensional immunocompetent intestine-on-chip model as *in vitro* platform for functional and microbial interaction studies

Michelle Maurer[a,c], Mark S. Gresnigt[b], Antonia Last[b], Tony Wollny[c], Florian Berlinghof[c], Rebecca Pospich[d,e], Zoltan Cseresnyes[f], Anna Medyukhina[f], Katja Graf[b], Marko Gröger[a,g], Martin Raasch[a,c], Fatina Siwczak[a], Sandor Nietzsche[i], Ilse D. Jacobsen[a,d,h], Marc Thilo Figge[f,h], Bernhard Hube[b,h], Otmar Huber[a,c], Alexander S. Mosig[a,c,*]

[a] Center for Sepsis Control and Care, Jena University Hospital, Friedrich-Schiller-University of Jena, Jena, Germany
[b] Department of Microbial Pathogenicity Mechanisms, Leibniz Institute for Natural Product Research and Infection Biology - Hans-Knoell-Institute, Jena, Germany
[c] Institute of Biochemistry II, Jena University Hospital, Jena, Germany
[d] Research Group Microbial Immunology, Leibniz Institute for Natural Product Research and Infection Biology-Hans Knoell Institute, Jena, Germany
[e] Division of Immunodermatology and Allergy Research, Hannover Medical School, Hannover, Germany
[f] Research Group Applied Systems Biology, Leibniz Institute for Natural Product Research and Infection Biology (HKI), Jena, Germany
[g] University of California, UCSF Broad Center of Regeneration Medicine and Stem Cell Research, San Francisco, USA
[h] Institute of Microbiology, Faculty of Biological Sciences, Friedrich Schiller University, Jena, Germany
[i] Centre for Electron Microscopy, Jena University Hospital, Friedrich-Schiller-University of Jena, Jena, Germany

ARTICLE INFO

Keywords:
Microphysiological system
Gut-on-chip
Microbiota
Mucosal immunity
Candida albicans
Lactobacilli

ABSTRACT

Alterations of the microbial composition in the gut and the concomitant dysregulation of the mucosal immune response are associated with the pathogenesis of opportunistic infections, chronic inflammation, and inflammatory bowel disease. To create a platform for the investigation of the underlying mechanisms, we established a three-dimensional microphysiological model of the human intestine. This model resembles organotypic microanatomical structures and includes tissue resident innate immune cells exhibiting features of mucosal macrophages and dendritic cells. The model displays the physiological immune tolerance of the intestinal lumen to microbial-associated molecular patterns and can, therefore, be colonised with living microorganisms. Functional studies on microbial interaction between probiotic *Lactobacillus rhamnosus* and the opportunistic pathogen *Candida albicans* show that pre-colonization of the intestinal lumen of the model by *L. rhamnosus* reduces *C. albicans*-induced tissue damage, lowers its translocation, and limits fungal burden. We demonstrate that microbial interactions can be efficiently investigated using the *in vitro* model creating a more physiological and immunocompetent microenvironment. The intestinal model allows a detailed characterisation of the immune response, microbial pathogenicity mechanisms, and quantification of cellular dysfunction attributed to alterations in the microbial composition.

1. Introduction

Commensal microorganisms of the intestinal microbiota support the digestion and absorption of nutrients by the gut. Microbial colonization is supported by the host *via* a mucus layer secreted by epithelial cells organized in a complex tissue comprising villi and crypts that form a tight and protective barrier between the microbiota and the circulation. A physiological communication between the members of the intestinal microbiota and their host is crucial for the maintenance of homeostasis in the human body. Thus, dysregulation and imbalance of these interactions known as dysbiosis are directly associated with the development of human diseases, including diabetes [1], obesity [2], inflammatory bowel disease (IBD) [3], cancer [3], depression [4] and non-infectious inflammatory diseases caused by opportunistic pathogenic fungi [5].

However, current knowledge on the impact of the microbiota on health is based solely on descriptive and correlative studies. So far, the lack of suitable experimental models prevented mechanistic studies on the complex cellular and molecular signalling processes within the microbiota under physiological conditions. Current *in vitro* models lack

* Corresponding author. ASM Center for Sepsis Control and Care, Jena University Hospital, Friedrich-Schiller-University of Jena, Jena, Germany.
E-mail address: alexander.mosig@med.uni-jena.de (A.S. Mosig).

https://doi.org/10.1016/j.biomaterials.2019.119396
Received 14 May 2019; Received in revised form 8 July 2019; Accepted 28 July 2019
Available online 02 August 2019
0142-9612/

the required tissue complexity with major limitations for the co-culture of living bacteria with human intestinal cells. On the other hand, animal models have limitations in the transferability to the human situation, since the composition of the microbiota, as well as immune system considerably varies between men and mice and even between individual mouse strains [6]. Established cell lines, such as Caco-2 cells, cultured as monolayers on extracellular matrix-coated standard plastic dishes or transwell inserts are frequently used to study human intestinal epithelial cells *in vitro*. Although these two-dimensional culture techniques have elucidated numerous aspects of intestinal epithelial cell biology, it should be noted that they do not recreate typical microanatomical structures of the human intestine.

The intestine is the primary site for interaction of the gut microbiota consisting of commensal microorganisms and opportunistic pathogens [7]. The continuous exposure to microbial-associated molecular patterns (MAMPs) in the intestinal lumen requires the immune system to weigh tolerogenic and protective responses continuously. It is becoming increasingly clear that dysregulation of this tolerant immune response and alterations in the gut microbiota contribute to chronic inflammatory diseases and breakdown of the gut barrier [3,8]. Although three-dimensional organoid cultures allow the *in vitro* differentiation of microanatomical structures in high detail [9], these models have limitations in their ability to reflect a tolerant immune response to the colonising microbiota. Recently a microfluidically perfused model of the human intestine has been described that allows circulation of peripheral blood mononuclear cells (PBMCs) and effectively recapitulates structural features of intestinal microanatomy and physiology, including a polarised intestinal tissue differentiation [10,11]. Although this system represents a major advancement in emulating the human intestine, models are still required that are capable of stably cultivating commensal microbiota in an immune responsive environment and consider the balanced response to the microbiota and its metabolites.

The Toll-like receptor 4 agonist lipopolysaccharide (LPS) derived from gram-negative bacteria is a ubiquitously present MAMP in the human intestinal lumen [12]. However, upon dysfunction of the intestinal barrier, LPS can translocate into the circulation and in more substantial amounts eventually triggers a systemic inflammatory response syndrome associated with multiple organ failure [13]. Phagocytes play a critical role in gatekeeping MAMPs between the intestinal lumen and the circulation. In mice, it has been shown that tissue-resident phagocytes such as mucosal macrophages (mMphs) and dendritic cells (DCs) are central players in the release of inflammatory cytokines [14]. Both cell types populate the normal human intestinal mucosa but play distinct complementary roles in the selective local immune response and tissue homeostasis with mMphs as the most abundant mononuclear phagocytes in the intestinal lamina propria [15]. They account for most of the uptake of microbes that cross the epithelial barrier and are required to maintain an anti-inflammatory milieu in the mucosa by scavenging of apoptotic and damaged cells [16,17]. The expression of G protein-coupled chemokine receptor CX3CR1 on mMphs has been demonstrated as a central receptor in regulating intestinal barrier integrity [18,19]. The homeostatic function of $CX3CR1^+$ mMphs is complemented by $CD103^+$ DCs that represent another primary antigen-presenting cell type of the intestine [20]. These cells continually sample their environment for antigens derived from food, microbiota, and self-antigens [21] by extension of transepithelial dendrites into the intestinal lumen [22]. During homeostasis, intestinal DCs are considered to be tolerogenic, whereas mMphs are actively involved in tissue remodelling.

To resemble these conditions *in vitro*, we developed a three-dimensional model of the human intestine composed of endothelial and epithelial cell layers forming organotypic microanatomical villus- and crypt-like structures. For the first time, we demonstrate physiological interactions between epithelial and endothelial cells in an immunocompetent environment. This is created by tissue resident mMphs and DCs in a microphysiological model resembling essential conditions within the human intestine. We studied the biological intestinal homeostasis, barrier functionality and immunotolerance to stimulation with LPS at the intestinal luminal side of the model. To emulate dysregulation, imbalance and inflammation, the endothelial side was stimulated with LPS in a model of endotoxemia. Furthermore, we colonized the intestinal model with non-damaging living bacteria (*Lactobacillus rhamnosus*). Similar to *in vivo,* where the intestinal microbiota antagonizes microbial associated pathogenicity by limiting overgrowth and translocation through the intestinal epithelial barrier, we validated *L. rhamnosus'* antagonistic interactions on the opportunistic pathogenic fungus *Candida albicans* in our intestinal model.

2. Material and methods

2.1. Cell isolation and culture

Endothelial cells: Human umbilical cord vein endothelial cells (HUVECs) were isolated and seeded at a density of 2.5×10^4 cells/cm^2 in Endothelial Cell Medium (ECM) (Promocell, Heidelberg, Germany) up to passage 4 as described previously [23]. The study was approved by the ethics committee of the Friedrich Schiller University Jena (2018–1052), and all donors were informed about the aim of the study and gave written consent.

Caco-2 cells: The human epithelial colorectal cell line Caco-2 was kindly provided by the Institute for Laboratory Medicine, Clinical Chemistry and Pathobiochemistry, Charité - University Medicine Berlin. Cells were cultured in DMEM (GIBCO Darmstadt, Germany) supplemented with 10% foetal calf serum (FCS, Life Technologies), 20 ng/ml gentamicin (Invitrogen), 1% MEM non-essential amino acids (GIBCO). 5×10^5 Caco-2 cells are seeded in a 25 cm^2 flask and cultured in DMEM medium (Life Technologies) containing 10% FCS. The medium was changed every three to four days and cells used from passage 30 to 50.

Peripheral blood mononuclear cells and primary macrophages: PBMCs of three different healthy donors were isolated by Ficoll density gradient centrifugation as described previously [66] and seeded in 6- well plates with a density of 1.0×10^6 cells/cm^2 in X–VIVO 15 medium (Lonza, Cologne, Germany) supplemented with 10% (v/v) autologous human serum, 10 ng/ml human granulocyte macrophage colony-stimulating factor (GM-CSF) (PeproTech, Hamburg, Germany), 10 ng/ml M-CSF (PeproTech), 100 U/ml penicillin and 100 µg/ml streptomycin (Pen/Strep) (Thermo Fisher, Darmstadt, Germany). After 1 h incubation in a humidified cell incubator at 5% CO_2 and 37 °C the cells were washed twice with X–VIVO 15 medium and cultivated for 24 h before subcultured with endothelial cells in the biochip were terminal macrophage differentiation was performed in the supplemented X–VIVO 15 medium.

2.2. Biochip cell culture

MOTiF biochips made from polystyrol (PS) were obtained from microfluidic ChipShop GmbH (Jena, Germany). Biochips were manufactured by injection moulding as described elsewhere [23]. The chamber above the membrane has a height of 700 µm; the chamber under the membrane has a height of 400 µm. The width of the afferent and efferent channels is 0.8 mm and 2 mm, respectively. The height of these channels is 0.6 mm and 0.4 mm, respectively. Upper and the lower chamber including channel systems have a volume of 220 µl and 120 µl, respectively. A 12 µm thin polyethylene terephthalate (PET) membrane with a pore diameter of 8 µm and a pore density of 1×10^5 pores/cm^2 (TRAKETCH Sabeu, Radeberg, Germany) was integrated. An area of 1,1 cm^2 is available for cell culture. Chips and channels structures were sealed on top and bottom side with an extruded 140 µm thin PS foil using a low-temperature proprietary bonding method. Gas permeable silicon tubing was used for perfusion allowing oxygen equilibration during experiments. Additionally, PS bulk material and 140 µm thin PS bonding foil allowed re-diffusion of oxygen. Ramping

structures have been introduced into the chip bulk for prevention of unfavourable flow conditions and trapping of stationary air bubbles. For hydrophilization of the whole surface, the biochips were treated with oxygen plasma.

Intestine-on-chip models were assembled by staggered seeding of endothelial and epithelial cell layers. HUVECs were seeded with a density of $1.5 \times 10^5\,cm^{-2}$ in the upper chamber of a sterilised biochip in EC medium. Following 48 h of culture, macrophages were seeded on top of the confluent HUVEC cell layer with a density of $5 \times 10^4\,cm^{-2}$ in M199 medium (Life Technologies) supplemented with 10% FCS), 10% (v/v) autologous serum, 68×10^{-7} M L-glutamine (Sigma-Aldrich), 25 µg/mL heparin (Sigma- Aldrich), 7.5 µg/ml endothelial mitogen (Thermo Fisher), 5 µg/ml ascorbic acid (Sigma-Aldrich), 10 ng/ml GM-CSF, 10 ng/ml M-CSF and Pen/Strep. After 72 h of static culture and daily medium exchange, Caco-2 cells were seeded in the bottom chamber of the biochip with a density of $4{,}5 \times 10^5\,cm^{-2}$ and cultured in DMEM. The inlets of each biochip were sealed and the whole intestinal model cultured upside down for 24 h under static conditions. Subsequently, the fully assembled organ-on-chip model was used in experimental series as described. The endothelial side of the model was perfused with M199 medium with a flow rate of 50 µl/min (shear stress: 0.07 Pa). The luminal side of the model was perfused with 50µl/min (shear stress: 0.01 Pa). For LPS stimulation cells were treated with 100 ng/ml LPS (Sigma-Aldrich, Taufkirchen, Germany). Supernatants were collected and replaced with fresh medium containing 100 ng/ml LPS after 24 h. Supernatants were collected again after an additional 24 h. Cells were cultured in a humidified cell incubator at 5% CO2 and 37 °C.

2.2.1. Microbial strains and culture conditions

L. rhamnosus ATCC 7469 was grown on Man, Rogosa, and Sharpe (MRS) agar plates (Carl Roth, Karlsruhe, Germany) at 37 °C and 1% O_2. For use in experiments, bacterial cells were grown at 37 °C without agitation in MRS broth (Carl Roth, Karlsruhe, Germany). Prior to experiments, lactobacilli were collected by centrifugation, washed twice in PBS and diluted to an optical density OD_{600nm} of 0,5 in DMEM.

The *C. albicans* wild-type strain SC5314 was grown on YPD plates (2% peptone, 1% yeast extract, 2% glucose, 2% agar) at 30 °C. For use in experiments, *C. albicans* cells were grown overnight (o/n) in YPD medium (2% peptone, 1% yeast extract, 2% glucose) at 30 °C and 180 rpm. Prior to infection, yeast cells from an o/n culture were collected by centrifugation, washed two times with phosphate-buffered saline (PBS), the cell number was determined using a Neubauer chamber system, and adjusted to 5×10^3 cells/120 µl in DMEM.

Host cells were cultured in antibiotic-free medium for 72 h. After 24 h of LPS treatment, the bacterial suspension was inoculated onto the epithelial layer and incubated for 30 min to allow attachment to the epithelium. Subsequently, unattached cells were removed and PBMCs inoculated. The endothelial layer was cyclically perfused with a flow-rate of 50µl/min (shear stress: 0.07Pa) while the luminal chamber was linearly perfused with 25µl/min (shear stress: 0.03Pa). After 24 h of culture in the chip, supernatants were plated on MRS agar (Carl Roth). The membrane was lysed in 0.2% Triton-X 100 for 15 min at RT and removed before the suspension was pelleted, washed with PBS and plated.

2.3. Immunofluorescence staining

Cells were fixed with either 4% paraformaldehyde for 10 min at room temperature or methanol for 20 min at −20 °C. For permeabilization and blocking of unspecific binding sites, cells were incubated in PBS including 0.1% saponin (Sigma Aldrich) and 3% goat serum (Dianova, Hamburg). Staining was performed with antibodies against CD68, CD103, E-cadherin, VE-cadherin, β-Catenin (BD Biosciences, Heidelberg, Germany), occludin, ZO-1 (Invitrogen, Karlsruhe, Germany), CEACAM-1, CX3CR1, CYP3A4 (Merck-Millipore, Schwalbach, Germany), α-defensin (abcam, Cambridge, UK), mucin 2 (Acris, Herford, Germany), villin (Santa Cruz Biotechnology, Heidelberg, Germany), von Willebrand factor (Dako, Hamburg, Germany) and secondary antibodies goat-anti-mouse-Cy3, goat-anti-rabbit-AF488, goat-anti-rabbit-AF647, DAPI (Invitrogen) and Phalloidin (ThermoFisher). Samples were embedded in fluorescent mounting medium (Dako). Imaging was performed with an AxioObserver Z1 fluorescence microscope equipped with an ApoTome-2 (Carl Zeiss AG, Jena, Germany). Images were analysed with ImageJ2 software (Fiji).

2.4. Scanning electron microscopy

Cells were fixed with 2.5% (v/v) glutaraldehyde in cacodylate buffer for 120 min. Afterwards, the samples were washed twice with cacodylate buffer for 10 min and dehydrated in ascending ethanol concentrations (30, 50, 70, 90 and 100%) for 10 min each. Subsequently, the samples were critical-point dried using liquid CO_2 and sputter coated with gold (thickness approx. 4 nm) using a SCD005 sputter coater (BAL-TEC, Liechtenstein) to avoid surface charging. Finally, the specimens were investigated with a field emission (FE) SEM LEO-1530 Gemini (Carl Zeiss NTS GmbH, Oberkochen, Germany).

2.5. Image analysis and quantification

Images were acquired as Z-stacks utilising a Zeiss Apotome microscope and were saved in the Zeiss native image format „CZI". The Apotome images were first processed by Zeiss' ZEN software to provide optical sectioning. Further preprocessing included deconvolution using Huygens Professional (SVI, Hilversum, Holland), applying the „Spinning disk" deconvolution module by setting the pinhole spacing at 4 µm, according to SVI guidelines. The deconvolved images were analysed using Imaris 9.2.1 (Bitplane, Zürich, Switzerland). Automated quantification of confocal fluorescence microscopy data was performed by customised software, which was implemented in the programming language "python" (https://www.python.org/) and is available upon request.

Cell-based analysis: The three-dimensional image data were used to identify individual cells applying nuclear staining as guidance. Here the „Cells" module of Imaris was applied, where the DAPI channel was selected to create the cell nuclei, whereas the E−(VE-) cadherin or the ZO-1 labelling channel provided information about the membrane location. The segmented nuclei served as seeds to assist the search for the cell membranes. After successful segmentation, the area between the nuclei and the cell membrane was identified as cytoplasm. Particle analysis was applied when necessary, where the intensity and morphometry of additional components (for example the von Willebrand factor) was characterised in the cytoplasmic area.

Membrane-based analysis: The 3D image stacks were preprocessed in Zen and Huygens Professional as described above. In analysing the (V) E-cadherin and ZO-1 distribution, cell membranes were segmented using the Surfaces module of Imaris 9.2.1. The deconvolved Z-stacks were locally thresholded using the Otsu algorithm with a 2-µm neighbourhood diameter preceded by Gaussian blurring with a spatial filter size of 0.4 µm. The segmented membrane objects were limited to items with sphericity in the range of 0.0–0.9 and volume above 100 voxels in order to exclude artefacts. Macrophages were segmented as surfaces objects in Imaris. Here the Gaussian blurring was executed with a filter size of 0.645 µm, and the local Otsu thresholding was applied at a 2.4-µm neighbourhood diameter. The macrophage volume was limited to the 60–1200 µm [3] range in order to avoid detecting fragments or large clusters.

Quantification: Statistical information was extracted from the segmented images in Imaris 9.2.1. Here we measured the mean and the standard deviation of the fluorescence intensity for all channels within all regions of the segmented surfaces and cells; the area, the volume and

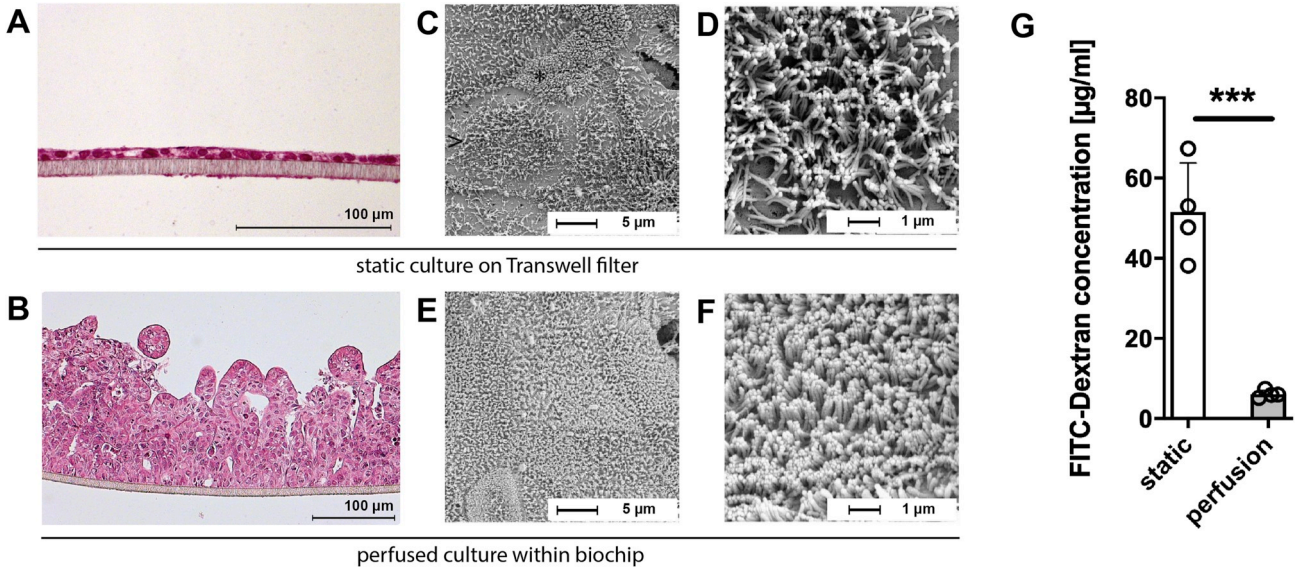

Fig. 1. Caco-2 cells form crypt and villus-like structures under perfusion conditions in the biochip. A, B) Histological H&E staining of Caco-2 cell layers cultured A) statically in the transwell, and B) under perfused conditions in the biochip. C-F) Scanning electron microscopy of Caco-2 cell layers cultured for 7 days under C, D) static conditions on transwell filters, and E, F) under perfusion conditions in the biochip. G) Permeability of epithelial cell layers for FITC-labelled dextran beads (3–5 kDa) under static and perfused conditions in the biochip. A-F) microscopy images are representative of three independent experiments, G) data from four independent experiments, data presentation shows the mean ± standard deviation., Statistical test was made using the Student's t-test, ****p < 0.0001.

the sphericity of the entire cells, the cell compartments and the cell membranes; the number of cells per Z-stack, etc. These analysis results were saved in Excel spreadsheets and used for statistical analysis and plotting.

Ellipticity index: The reconstructed surfaces were assigned a best-fitting ellipsoid in Imaris. According to the relationship amongst the main axis of the ellipsoid (a, b, c), we characterized the surfaces as prolate (a = b < c; cigar-shaped) and oblate (a < b = c; disk-shaped), by using the following indices:

$$e_{prolate} = \frac{2a^2}{a^2 + b^2} * \left(1 - \frac{a^2 + b^2}{2c^2}\right),$$

$$e_{oblate} = \frac{2b^2}{b^2 + c^2} * \left(1 - \frac{2a^2}{b^2 + c^2}\right).$$

2D analysis: Automated quantification of VE-cadherin staining in 2D was performed by customized software, which was implemented in the programming language Python. Prior to the analysis, images were preprocessed with a median filter (size 3 pixels) to remove spike noise. Then each image was thresholded at 100 intensity levels (out of 255, 8-bit) to obtain a binary mask of the cellular junctions. After that, connected regions were identified and regions with an area less than 20 µm [2] were assigned to a separate class of small particles. To evaluate the integrity of the cellular junctions, we computed the total area of cellular junctions, as well as the mean and maximum intensity of the cellular junctions. For computing the mean intensity, only those pixels were used that belonged to the foreground after the thresholding step. Moreover, we computed the total area and area fraction of the small particles. In the latter case, the area of the small particles was normalized by the total area of the cellular junctions.

2.6. Cytokine profiles

Supernatants were collected after indicated time periods and immediately frozen at −80 °C. Cytokines were detected using CBA assay (BD Biosciences) according to the manufacturer's protocol. Enhanced sensitivity flex set was used for the measurement of TNF and IL-1β release. Secretion of IL-6, IL-8 and IL-10 was analysed using standard CBA flex sets. The analysis was performed on a BD FACS-Canto II cytometer with FACSDiva software. Data analysis was performed using FCAP Array V3 software (Softflow, Pecs, Hungary).

2.7. Permeability assay

Fluorescein isothiocyanate (FITC)-dextran (Sigma-Aldrich) with an atomic mass of 3–5 kDa was used. The medium in both chambers is replaced by preheated PBS. Subsequently, 150 µl FITC-dextran solution is added in the lower chamber containing Caco-2 cells and is incubated for 30 min at 37 °C. The biochip is turned upside down during incubation allowing FITC-dextran to permeate through the cell layer under static conditions. After washing of the lower chamber with PBS, the solution was collected from the upper chamber. All steps were performed protected from light.

2.8. Statistics

For each experiment replicates have been performed as indicated in the figure legend. Statistical analysis has been performed with GraphPad Prism 6.05 (GraphPad Software, La Jolla, CA, USA). For analysis of statistical significance, the tests indicated in the figure legend have been performed. A p-value < 0.05 was considered statistically significant.

3. Results

The epithelial cell layer of the intestinal model is formed by Caco-2 cells cultured on a 10 µm thin porous polyethylene terephthalate (PET) membrane suspended in the biochip and continuously perfused with cell culture medium. During cell culture, microfluidic perfusion ensures a constant removal of metabolic waste products and a continuous resupply with nutrients [23]. In contrast to conventional cell culture approaches such as transwell filters (Fig. 1 A), Caco-2 cells cultured in microfluidically perfused biochips form a self-organised three-dimensional cell layer with columnar epithelium (Fig. 2 B) and increased microvilli formation at the apical cell surface within 7 days of culture (Fig. 1C - F). Permeability measurements confirmed an increased barrier function of the three-dimensional cell layer compared to conventional cell culture under static conditions where only two-

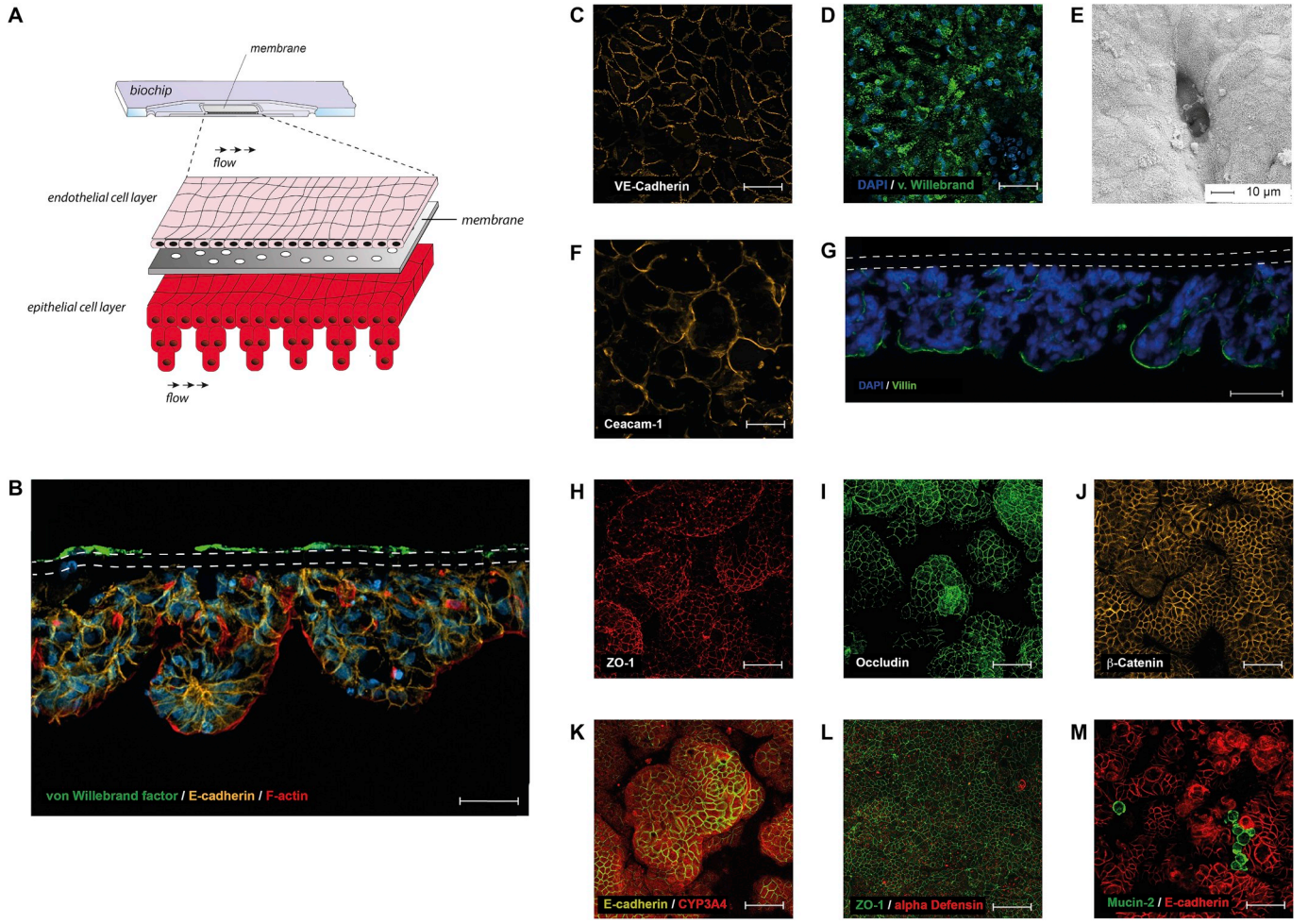

Fig. 2. Design of the intestine-on-chip model featuring organotypic microanatomy and expression of endothelial and intestinal epithelial cell type markers. A) A porous membrane suspended in the biochip serves as a scaffold for the multi-layered intestinal model composed of endothelial and epithelial cells. Microchannels integrated into the biochip separately perfuse both epithelial and endothelial layers at 50 µl/min. B) Cross-section of the three-dimensional intestinal model: endothelial cells express von Willebrand factor (green), epithelial cells express E-cadherin (orange) and F-actin (red). Both cell layers are separated by a porous membrane (dashed line). Actin filaments are stained with phalloidin (red). Scale bar 100 µm. Nuclei were stained with DAPI (blue). C-D) Endothelial cells form a confluent monolayer and express C) VE-cadherin (orange) and D) von Willebrand factor (green). E-N) Epithelial cell layer: E) Scanning electron microscopic image of the crypt-like structures. Expression of F) CEACAM-1 (orange); G) villin (green) (DAP blue, dashed lines marks membrane); H) ZO-1 (red); I) occludin (green); J) β-catenin (orange); K) E-cadherin (orange); CYP3A4 (red); L) α-defensin (red); ZO-1 (green); M) mucin-2 (green); E-cadherin (red); C-D, F-J) Scale bar 50 µm. Nuclei were stained with DAPI (blue). C-M) Representative images of four independent experiments. (For interpretation of the references to color in this figure legend, the reader is referred to the Web version of this article.)

dimensional Caco-2 monolayers are formed (Fig. 1G).

The multi-layered tissue model was separately perfused by two microchannels at the endothelial and the luminal side of the model (Fig. 2A). The vasculature of the intestine was mimicked by co-culture of HUVECs on the membrane opposite to the epithelial layer. Endothelial cells formed a confluent lining in the biochip that express endothelial cell marker proteins VE-cadherin (Supplementary Video S1) and von Willebrand factor (vWF) (Fig. 2B–D). In the epithelial cell layer, we observed the cellular self-organisation into three-dimensional structures with morphological features of crypts and villi that fully cover the membrane serving as cell substrate (Fig. 2 E-J, Supplementary Video S2). The formation of a three-dimensional Caco-2 cell layer upon microfluidic perfusion has also been reported by Ingber and colleagues, demonstrating the differentiation of these cells into a polarized columnar epithelium that contains cells with markers of absorptive, mucus-secretory, enteroendocrine, and Paneth cell populations [11]. Also in our model, villus-like structures appear polarised and express at the outer cell borders the carcinoembryonic antigen-related cell adhesion molecule 1 (CEACAM1, Fig. 2 F), a protein expressed by intestinal epithelial cells (IEC) *in vivo* at the apical surface of intestinal villi [24]. Further, villin, a protein controlling the shape and motility of IEC by interconnecting the brush borders to the cytoskeleton [25] was found expressed at the tip of villus-like structures (Fig. 2 G). These structures present themselves in a well-defined organisation expressing tight junction proteins ZO-1 and occludin (Fig. 2H, I), both critically involved in the maintenance of barrier function [26]. Further, β-catenin (Fig. 2 J), an essential regulator of epithelial cell proliferation and differentiation [27], and cytochrome P450 3A4 (CYP3A4, Fig. 2 K), a major CYP enzyme responsible for metabolizing over fifty percent of prescribed drugs [28] are stably expressed by the epithelial cell layer. In contrast to static culture, Caco-2 cells differentiate under perfusion conditions into cell-subtypes expressing specific cell type markers such as α-defensin, a marker of Paneth cells (Fig. 2 L) and Mucin-2, a marker protein of Goblet cells (Fig. 2M).

Supplementary video related to this article can be found at https://doi.org/10.1016/j.biomaterials.2019.119396

The lack of tissue-resident mMphs and DCs is a limitation of most currently available *in vitro* gut models. These two cell types are required to initiate immune responses causing inflammation and to prevent pathogen dissemination, yet also for mediation of immunotolerance to

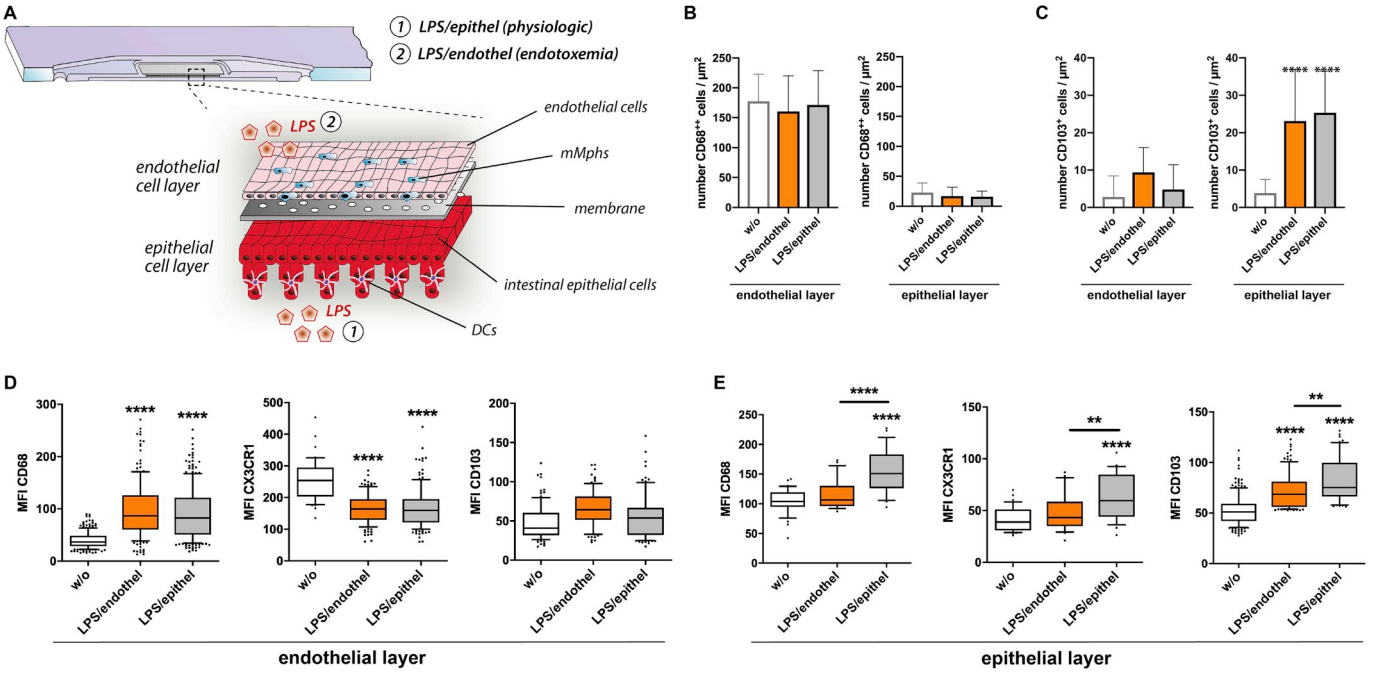

Fig. 3. Mobility and phenotype marker expression of mPCs upon LPS stimulation. A) The distribution pattern of mPCs with the majority of mMphs populating the endothelial cell layer and DCs residing in the epithelial cell layer. Two different LPS stimulation conditions were tested for recreating 1) physiological contact of epithelial cells with LPS; and 2) conditions of endotoxemia, with LPS exposed to the endothelial cell layer. B-C) Total number of B) $CD68^{++}$ cells or C) $CD103^{+}$ cells per µm [2] within the endothelial or epithelial cell layer of the non-stimulated model (w/o), and the model stimulated at the endothelial side (LPS/endothel) or the epithelial side (LPS/epithel). D-E) Mean fluorescence intensity (MFI) of CD68, CX3CR1 and CD103 expression by mPCs in the D) endothelial and E) epithelial cell layer. Whisker plots: 10th – 90th percentile, the box represents the 25th and 75th percentile with the line in the box marking the median. Data points outside whiskers mark outliers. A-D) Statistical testing with one-way ANOVA and Tukey's correction, $^{**}p < 0.01$, $^{****}p < 0.0001$ vs. non-stimulated condition (w/o); Data of five independent experiments is shown.

commensal bacteria and derived MAMPs in the gut lumen. To simulate these functions *in vitro*, human primary monocytes were seeded on the endothelial cell layer and differentiated in the presence of macrophage colony stimulating factor (M-CSF), and granulocyte-monocyte colony stimulated factor (GM-CSF). After 7 days of culture, monocytes differentiated into two phenotypically distinct monocyte-derived phagocyte subsets (mPCs) resembling features of mMphs and DCs, respectively. The functionality of these mPCs was studied in the presence of LPS, both at the endothelial and epithelial cell layer (Fig. 3 A). Expression of CX3CR1 with a high level of CD68 ($CD68++$) defined mMph surrogates, whereas DCs were defined by expression of lower CD68 levels ($CD68^{+}$) and the presence of the DC marker integrin alpha E (CD103). It has been reported that mMphs depend on CX3CR1 to be maintained within the lamina propria and to prevent translocation of commensal bacteria to mesenteric lymph nodes [29]. In accordance with these reports, we found that LPS exposure to the intestinal luminal side of the model triggered mMphs and DCs to self-organise within the tissue. LPS stimulation at the intestinal luminal side supported the formation of $CD68^{+}/CD103^{+}$ DCs and triggered DC invasion into the epithelial cell layer (Fig. 3C, D, E) with some of these DCs forming dendrites through the epithelial cell layer contacting the luminal space (Supplementary Figure 1). In mice, lamina propria-resident $CD103^{+}$ DCs were shown to migrate into the epithelium during homeostasis to facilitate capture of bacterial antigens [21]. In the intestinal model, a significantly increased expression of CD103 by DCs was observed at the luminal side upon epithelial cell stimulation (Fig. 3 D, E, Supplementary Figures 2 and 3). Thus, a physiological contact of epithelial cells with LPS contributed to improved DC maturation within the epithelial cell layer. LPS stimulation also upregulated CD68 and CX3CR1 in mMphs that predominately populate the endothelial cell layer (Fig. 3 B, D, E).

Endotoxemia represents a disease condition in which LPS leaks into the bloodstream. This condition was simulated by exposing the endothelial lining to LPS. Although we observed an upregulation of CD68 in mPCs, we were unable to find increased upregulation of CX3CR1 in mMphs within the epithelial cell layer as observed upon intestinal luminal LPS stimulation. Further, CD103 expression by DCs was significantly decreased in the epithelial barrier compared to LPS stimulation at the luminal side (Fig. 3 B - E). These results demonstrate guided mobility and adapted activation pattern of mPCs depending on the microenvironment created by the endothelial and epithelial cell layers with their individual responsiveness to LPS exposure.

Subsequently, we studied the responsiveness of mPCs depending on their differentiation and distribution pattern induced by the different LPS stimulation sites. In general, no adverse effects were observed on barrier functionality despite the presence of mPCs in the model, irrespective of the side of LPS exposure (Fig. 4 A). Under simulated physiological conditions with LPS present at the luminal side of the model, we observed immunotolerance reflected by the absence of a release of pro-inflammatory cytokines. However, emulated endotoxemia with LPS exposure to the endothelial layer induced a robust inflammatory response characterized by release of TNF, IL-1β, IL-6, and IL-8 (Fig. 4B–E).

The proinflammatory cytokines TNF, IL-1β, IL-6, and IL-8, are essential mediators of human intestinal inflammation and LPS-induced cell damage [30]. Moreover, these cytokines are critically involved in the loss of intestinal barrier function frequently observed in IBD [31,32]. A decrease in the expression of endothelial VE-cadherin, and E-cadherin/ZO-1 expressed by IECs is directly associated with intestinal permeability in IBD [33]. Similar observations were made in our intestinal model, were direct exposure of the endothelial lining to LPS significantly reduced expression of VE-cadherin with a diffuse and disrupted expression pattern along the cell borders. In addition, an analysis of endothelial cells by quantification of the cellular ellipsoid index (0 = line, 1 = circle) revealed significant morphological

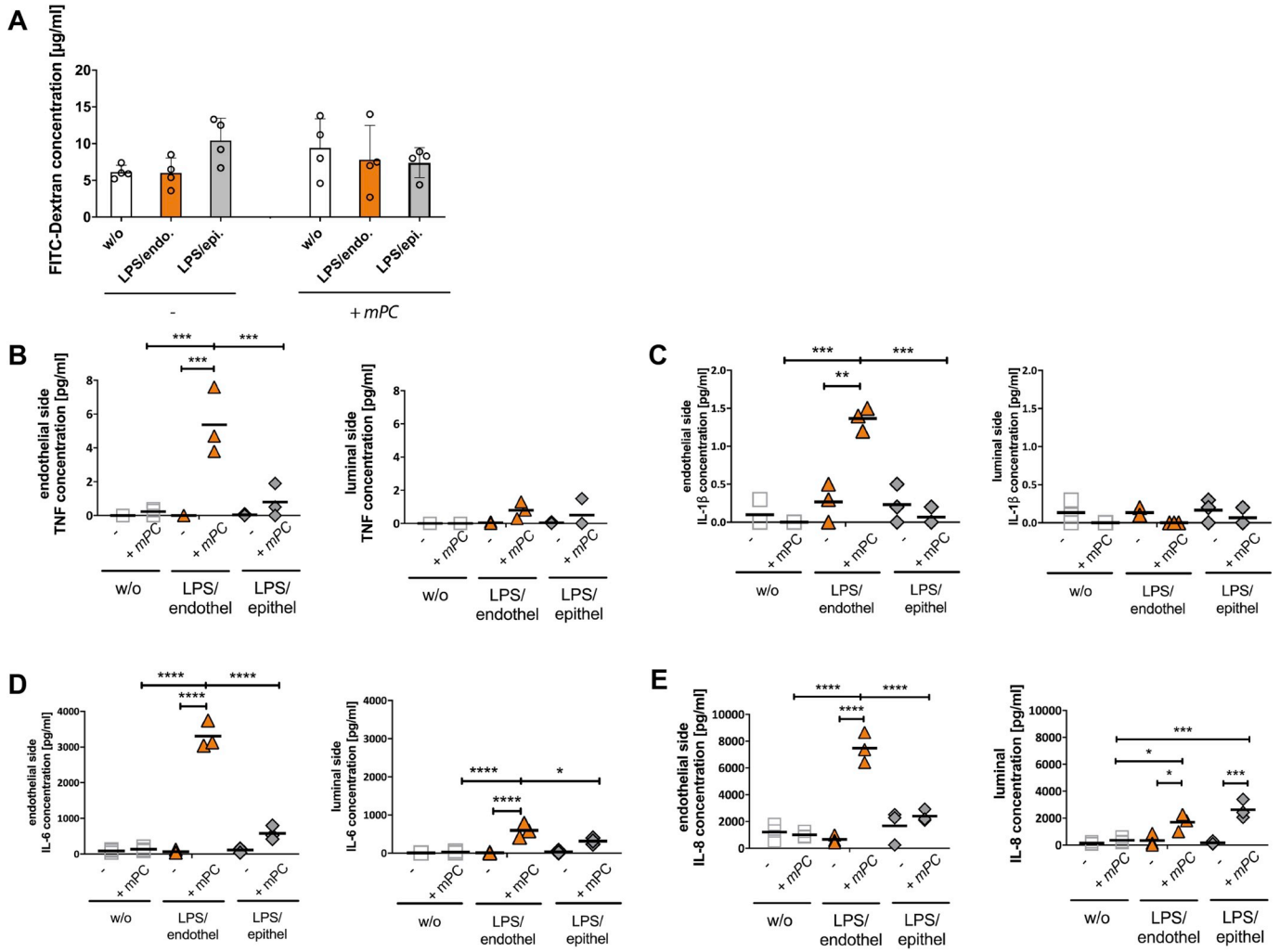

Fig. 4. Permeability and cytokine release upon LPS stimulation. A) Permeability of the intestinal model for FITC-dextran, and B-E) release of proinflammatory cytokines B) TNF, C) IL-1β, D) IL-6, and E) IL-8 at the endothelial or luminal side of the intestinal model without LPS stimulation (w/o), and upon LPS stimulation at the endothelial cell layer (LPS/endothel) or the epithelial cell layer (LPS/epithel) in absence (−) or presence (+) of mPCs. B-E) data is shown as scatter plots with mean values ± standard deviation, statistical significance was calculated by two-way ANOVA with Sidak's multiple comparisons test (****$p < 0.0001$; ***$p < 0.001$; **$p < 0.01$; *$p < 0.05$). Data of three independent experiments are shown.

alterations of endothelial cells directly exposed to LPS. Endothelial cells exposed to LPS appeared elongated with a diffuse VE-cadherin expression, indicating endothelial dysfunction [34]. In contrast, we observed an even increased VE-cadherin expression and no alterations of endothelial morphology when LPS was perfused at the intestinal lumen of the model (Fig. 5A and B; Supplementary Figure 4). Similar observations were made for E-cadherin and ZO-1 expression in the epithelial cell layer. For both proteins, we found an increased expression level when the epithelial cell layer was stimulated with LPS. However, the expression of E-cadherin and ZO-1 was significantly reduced when the endothelial cell layer was exposed to LPS (Fig. 5C, D; Supplementary Figs. 4B and C).

The observed immunotolerance at the luminal side represents a crucial physiological feature required for stable colonisation with living bacteria in the presence of functional mPCs. Therefore, we next colonised the luminal side with the probiotic bacterium *L. rhamnosus* in the presence of LPS at the luminal side resembling physiological conditions. Alternatively, LPS was added to the endothelial layer mimicking endotoxemia. We observed that independent from the side of LPS stimulation, *L. rhamnosus* stably colonised the epithelial cell layer without translocating through the tissue barrier (Fig. 6 A). Further, a trend towards an improved barrier function was observed upon luminal colonisation with *L. rhamnosus* (Fig. 6 B). Infection of the intestinal tract is often accompanied by infiltration of the intestine by leukocytes [35]. We therefore introduced circulating PBMCs into the vascular perfusion circuit of the endothelial compartment to investigate the potential immunomodulatory effects of *L. rhamnosus* in the intestinal model. Measurement of the cytokine release profiles for IL-1β, IL-6, IL-8, IL-10, and TNF in intestinal models colonised with *L. rhamnosus* showed a significant increase of cytokine release and PBMC adhesion upon LPS stimulation of the endothelial cell layer compared to LPS stimulation at the luminal side (Fig. 6C, D). Though, we observed only slightly increased IL-1β and IL-6 levels and no alterations of IL-8, IL-10 and TNF release associated with the luminal colonisation with *L. rhamnosus*.

L. rhamnosus was described among other probiotic bacteria to reduce enteric colonisation and infection with opportunistic pathogens. Multiple mechanisms, including nutritional competition, reduction of barrier permeability, and the modulation of the immune response have been discussed in this context [36,37]. We found that *L. rhamnosus* colonisation significantly increased the expression of E-cadherin and ZO-1 even in the presence of PBMCs (Fig. 6 E, F) and improved cell viability at the epithelial cell layer indicated by lower LDH release (Fig. 6 G). Lactobacilli have been shown to counteract infections of the gastrointestinal tract (GI) by opportunistic pathogens [38,39]. The

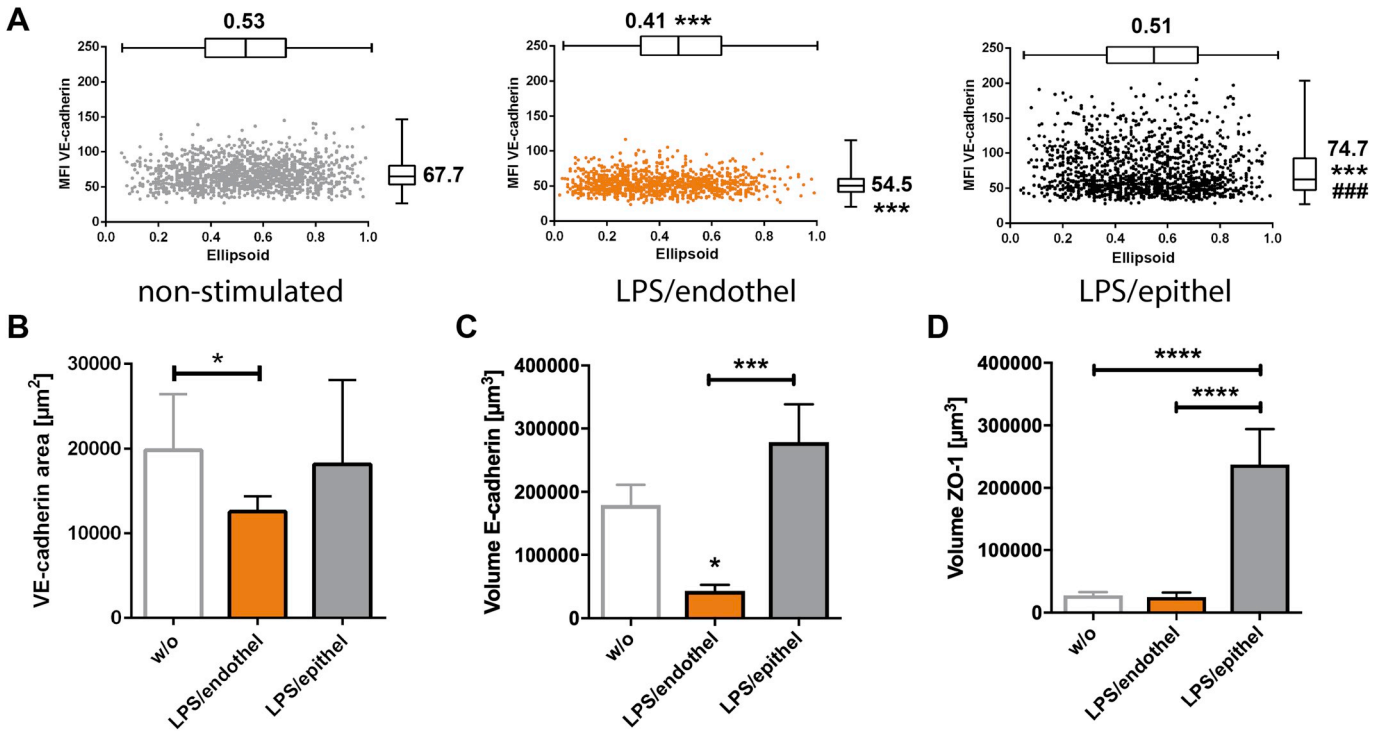

Fig. 5. Expression of VE-cadherin, E-cadherin and ZO-1 upon LPS stimulation. A) Expression pattern of VE-cadherin and endothelial cell morphology under non-stimulated conditions, and upon exposure of the endothelial layer to LPS (LPS/endothel) or the epithelial cell layer (LPS/epithel). Mean fluorescence intensity (MFI) of VE-cadherin expression is plotted for each individual cell analysed against its ellipsoid index (0 = line, 1 = circle). B) Quantification of VE-cadherin expression area in endothelial cells. C) Expression of E-cadherin and D) ZO-1 in the epithelial cell layers by z-stack image analysis and quantification as the volume of expressed protein levels. Statistical testing performed by one-way ANOVA with Tukey's correction; *p < 0.05, ***p < 0.001, ****p < 0.0001 vs. non-stimulated condition (w/o) or between indicated conditions. Data of four independent experiments are shown.

yeast *C. albicans* usually exists as a harmless commensal in healthy individuals [40]. However, it can also become a pathogen causing severe systemic infections as part of ultra-low diversity microbial communities in the gut, i.e. after antibiotic treatment of critically ill patients with suppressed immune function [41]. *L. rhamnosus* has been shown to interfere with colonization of *C. albicans* in the gut by limiting fungal growth [38,42]. However, most of these studies were performed in absence of epithelial cells [43,44] or in monolayered epithelial cell cultures [45–47]. We therefore studied the interaction of *C. albicans* with *L. rhamnosus* a more complex and immunocompetent microenvironment reflected by the intestine-on-chip model. The luminal side of the intestinal model was infected with *C. albicans*, and the impact of *L. rhamnosus* pre-colonization was analysed for the resulting fungal burden after 24 h of co-culture. We found that *L. rhamnosus* colonisation not only limit the growth of *C. albicans* at the luminal side of the model (Fig. 6H), but also reduces the translocation of the fungus over the intestinal barrier into the endothelial compartment emulating the vasculature (Fig. 6 I, J, K).

4. Discussion

The intestinal epithelium is one of the most dynamic and rapidly renewing tissues in the body, which requires continuous remodelling as well as disposal of effete cells. In order to simulate the human intestine as a stable and immunocompetent ecosystem, we developed a microfluidic organ-on-chip model forming a three-dimensional epithelial cell layer that can be colonised by living bacteria. We could demonstrate that the model, in contrast to monolayer cultures, exhibits near physiological 3D tissue architecture. Similar to normal intestinal epithelial our model demonstrates immunotolerance of resident mMphs and DCs to MAMPs (LPS) present in the intestinal lumen, whereas the presence of LPS in the vascular compartment elicited strong inflammatory responses. Further, we were able to include an artificial microbiota consisting of living lactobacilli that was shown to protect against invasion of the opportunistic pathogen *C. albicans* by lowering fungal burden overgrowth in the intestinal lumen and limiting fungal translocation through the gut barrier. Our observations are in agreement with reports from *in vivo* studies [38] and demonstrate the usefulness of the intestine-on-chip model as a platform for functional studies on microbial communication and host-microbe interaction *in vitro*.

A potential limitation of our model is the use of the intestinal epithelial Caco-2 cell line, isolated from a colorectal tumour [48]. However, the cell line was shown to exhibit features more similar to human small intestine [10,11] and to retain stem cell-like capabilities able to recreate microanatomical structures of the human intestine *in vitro* [11]. Caco-2 cells cultured under microfluidically perfused conditions can self-organise and differentiate into a polarised columnar epithelium containing cells with markers of absorptive, mucus-secretory, enteroendocrine, and Paneth cell populations [11], which is not observed in Caco-2 cells cultured under static conditions [49]. The use of perfused conditions is thus imperative to evolve a more physiological microenvironment facilitating proper cell differentiation and increased mucus secretion to provide a suitable substrate layer that could be efficiently populated by living bacteria. Moreover, microfluidic perfusion and related shear forces on cell layers have been recently shown to prevent detrimental bacterial overgrowth *in vitro* [50].

Recently the HuMiX system, a multichannel intestine chip consisting of Caco-2 cells has been described [51]. This system allowed substantial advances in modelling host-microbe interactions *in vitro* but lacks endothelial cells and an immunocompetent environment created by mPCs. Further, microorganisms cultured in the chip are separated by a nanoporous membrane from the epithelial cells preventing their direct interaction. To fully mimic host-microbe interaction direct interactions of epithelial cells, immune cells, and the microbes are required.

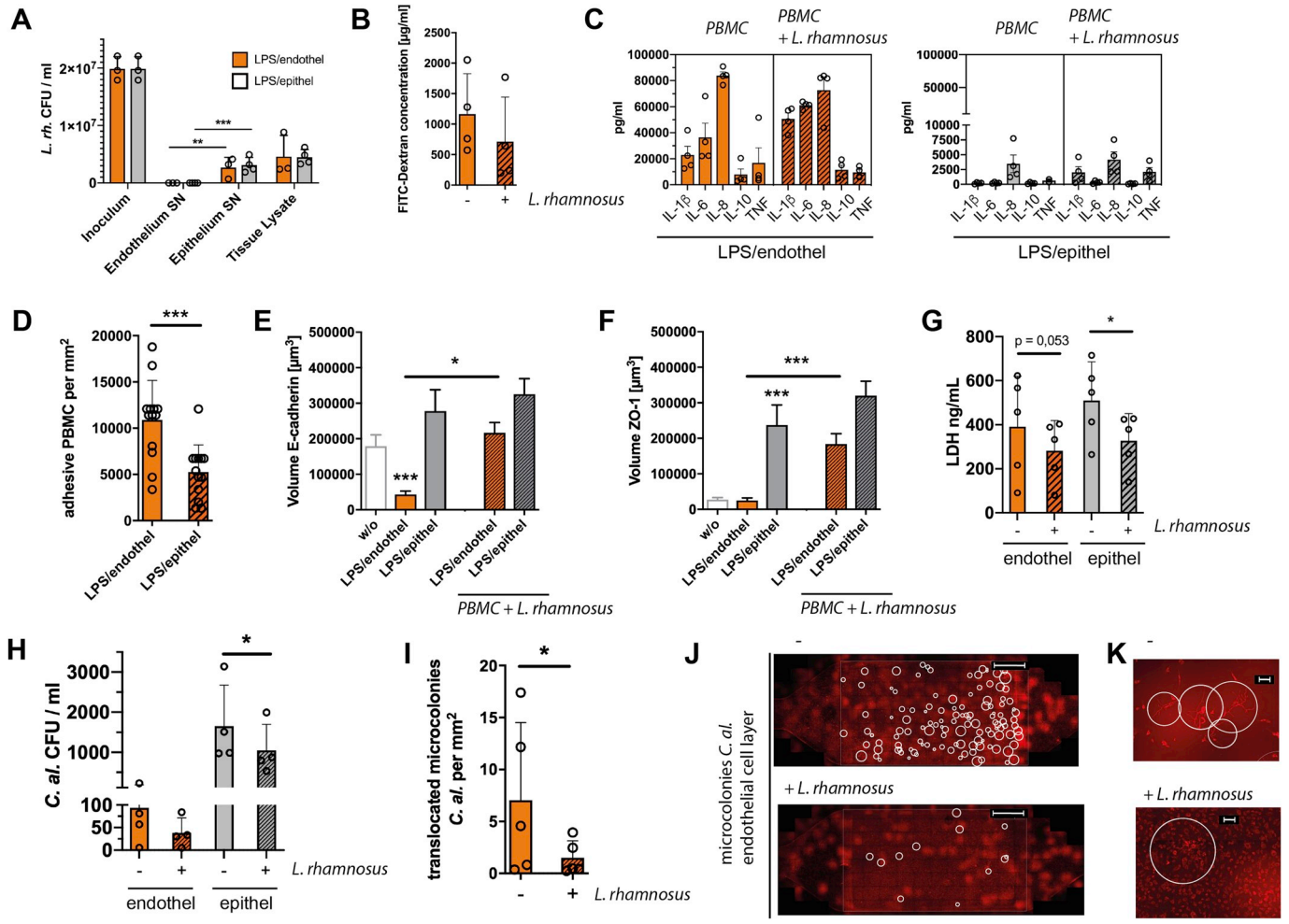

Fig. 6. Colonisation of the intestinal model with *L. rhamnosus* and *C. albicans*. A) Colony forming units (CFU) of *L. rhamnosus* from inoculated medium (Inoculum), in the supernatant at the endothelial side (Endothelium SN) or the luminal side (Epithelium SN), and in both cell layers after tissue lysis (Tissue Lysate). Colonisation was performed with LPS exposed to the endothelial side (LPS/endothel, orange bars) or LPS exposed to the epithelial cell layer (LPS/epithel, grey bars). B) Permeability assays with FITC-dextran in the model without *L. rhamnosus* (−) or *L. rhamnosus* colonised at the luminal side (+). C) Cytokine release in the supernatant at the endothelial side with endothelial cells stimulated with LPS (LPS/endothel) or epithelial cells stimulated with LPS (LPS/epithel). PBMCs were circulated at the endothelial side without *L. rhamnosus* (PBMC), and with *L. rhamnosus* colonising the luminal side of the model (PBMC + *L. rhamnosus*). D) Adhesive PBMCs in the presence of *L. rhamnosus* at the luminal side upon stimulation with LPS at the endothelial (LPS/endothel) or epithelial cell layer (LPS/epithel). E-F) Expression of E) E-cadherin and F) ZO-1 quantified as the volume in the epithelial cell layer. G) Release of LDH in the supernatant of the intestinal luminal side and vascular side with and without *L. rhamnosus* colonisation. H) Colony forming units (CFU) of *C. albicans* (*C. a.*) co-cultured without and with *L. rhamnosus* at the epithelial and endothelial side. I-K) C. Microcolonies formed by *C. albicans* upon translocation from the luminal side in absence or presence of *L. rhamnosus*. I) Quantified results of microcolony formation. J) low (scale bar 2 mm) and K) higher magnification (scale bar 100 µm) of formed microcolonies. J, K) Representative images of four independent experiments. Circles indicate identified microcolonies, fuzzy red background is caused by endothelial cells. E-F) A-C) Statistical testing with one-way ANOVA and Tukey's correction, *p < 0.05, ***p < 0.001 vs. non-stimulated condition (w/o) or between indicated conditions. D, G, H, I) Two-tailed ratio paired *t*-Test, *p < 0.05, ***p < 0.001 between indicated conditions. (For interpretation of the references to color in this figure legend, the reader is referred to the Web version of this article.)

The self-formation of the three-dimensional epithelial cell layer in our model allows the colonisation of living microorganisms directly at the luminal side of the intestinal model. Further, the organotypic microenvironment supports the self-organization of mMphs and DCs guided by physiological LPS gradients ranging from the luminal to the vascular side. Already present at birth, mMphs share many characteristics with their monocyte-derived counterparts in the adult intestine including high-phagocytic activity [52]. These findings support the emerging view that instead of their origin, the location and the surrounding microenvironment determines the functions of tissue-resident macrophages [53,54]. After their arrival in the mucosa, invading monocytes undergo a process of local cell differentiation and acquire the expression of CX3CR1 and MHCII [55]. During homeostasis, resident intestinal mMphs are replenished continuously by circulating monocytes with up to 50% of mature mMphs [56]. Similar to the *in vivo* situation these cells were found to express high levels of CX3CR1 upon LPS stimulation of the intestinal lumen. These mMphs primarily populated the endothelial side of the model, whereas CD103 expressing DCs were mainly recruited to the luminal side of the epithelial cell layer [19,21]. *In vivo* CX3CR1$^+$ mMphs initiate innate and adaptive immune responses to fungi in the intestine via expression of c-type lectin receptors [57]. Furthermore, it has been recently shown that CX3CR1$^+$ mMphs are critically involved in limiting microbiota-induced intestinal inflammation. They promote tissue homeostasis by limiting expansion of microbe-specific T helper 1 (Th1) cells and support the generation of microbiota specific regulatory T-cells. Interestingly, this study also demonstrated that colonization with microbes that adhere to the epithelium can compensate for intestinal microbiota loss and activate homeostatic immunoregulatory mechanisms [19]. Under physiological conditions *in vivo* mMphs do not respond to inflammatory triggers such

as LPS allowing them to act as efficient scavengers without inducing inflammation that usually ensues upon encounter of MAMPs and would compromise intestinal homeostasis [58]. In the intestinal model, we could demonstrate that LPS is well tolerated at the luminal side of the model with physiological homeostasis in the presence of commensal *L. rhamnosus*.

The maintenance of epithelial integrity has been shown to rely on the function of mMphs and DCs that reduce epithelial susceptibility to inflammatory insults and drive intestinal epithelial cell renewal and differentiation [59,60]. Further, mMphs stimulate the differentiation of regulatory T-cells and thereby contribute to intestinal homeostasis [61]. Recruited monocytes can differentiate into mature mMphs under inflammatory conditions exerting repair functions as has been described for monocytes infiltrating the liver [62,63]. We were able to demonstrate that by integration of mMphs and DCs tissue homeostasis can by mediated and LPS is tolerated at the luminal model side. Further, primary leucocytes (PBMCs) can be perfused in the model in the presence of LPS without detrimental effects on immune cell activation.

Colonisation of the intestine with *L. rhamnosus* did not induce inflammatory responses by release of proinflammatory cytokines. Instead, colonization improved cell viability of the intestinal model and was associated with increased E-cadherin and ZO-1 expression in the epithelial layer under simulated conditions of endotoxemia. These observations are in agreement with recent *in vivo* studies in mice, were an improved E-cadherin expression was also induced by lactobacilli [36]. Although the mechanism of the barrier improvement remains speculative, a potential explanation might be cytoprotective induction of heat shock proteins that were reported to contribute to cell protection by modulation of tight junction protein expression [64]. Stable colonisation of an intestinal model with *L. rhamnosus* was also shown by Kim *at al* [10]. However, PBMCs circulated in the model caused injury of villi and the intestinal barrier through the release of IL-8 induced by LPS present at the luminal side [10]. Here we demonstrate that in presence of mMphs and DCs physiological immunotolerance to LPS can be established, without detrimental effects of immune cell activation. This allows endothelial PBMC perfusion and a stable co-culture of living bacteria and LPS at the luminal side of the model. A pro-inflammatory immune response associated with tissue damage was only observed in the endotoxemia model, with *L. rhamnosus* colonisation ameliorating inflammation-associated tissue damage.

In vivo, continuous checks and balances between immune tolerance and the induction of inflammatory responses upon translocation of microorganisms are required. We observed increased leukocyte recruitment to the endothelial cell layer when LPS was present at the vascular side of the model creating an inflammatory environment that resembles conditions of IBD. The number of adhesive PBMCs under these simulated disease conditions was significantly higher compared to the more physiological conditions when LPS was present at the luminal side of the model. These observations are in agreement with clinical reports from IBD patients where blockade of recruitment of leucocytes into the intestine represents a promising treatment option for the patient [65]. The model has proven a suitable platform to elucidate mechanisms of host-microbe interactions in an immunocompetent environment in studies on leucocyte recruitment, immune cell differentiation, and the establishment of an adapted immune response to commensal and pathogenic microorganisms. Nevertheless, further improvements will be performed in follow up studies. These improvements should consider the contribution of other immune cells on immune surveillance of microorganisms in the gut, i.e. B- and T-cells organised in lymphoid follicles of the Peyer's patches and within gut-associated lymphoid tissue.

We could further demonstrate the feasibility of our model to investigate microbial interactions between commensal and opportunistic microorganisms with functional consequences for the intestinal barrier under near-physiological and well-controlled conditions *in vitro*. We here show for the first time that *L. rhamnosus* colonisation can diminish invasion of *C. albicans* into the “bloodstream” in a microphysiological environment created by our intestine-on-chip system. Similar to the *in vivo* situation where the bacterial microbiota protects against *C. albicans* overgrowth [38,39], we could demonstrate a protective effect of probiotic *L. rhamnosus* limiting the overgrowth and translocation of *C. albicans* to the endothelial cell compartment. It is tempting to speculate that also luminal exposure to LPS contributes to a reduced translocation of pathogenic microbes into the vascular compartment by improving the intestinal barrier.

Our intestinal model has proven to be a valuable tool to systematically explore the underlying mechanisms of microbial communication, host-microbe interactions, microbial pathogenicity mechanisms, and immune cell activation under physiologically relevant conditions *in vitro*. Thus, it represents a powerful platform for the investigation of disease mechanisms, driven by (opportunistic) pathogens, i.e. under well-defined conditions of dysbiosis created in synthetic microbiomes that are composed of a limited number of microbial community members. Further, it allows the screening and development of novel treatment strategies for IBD by supporting and maintaining physiological conditions of the human microbiota that keep opportunistic pathogens in their commensal state and prevent the onset of related inflammatory diseases.

Author contributions

M.M., T.W., F.B., M.G., M.R., F.S. contributed experiments for organ-on-chip development. M.M., M.S.G., A.L., R.P., K.G. contributed microbiological experimentation and functional interaction studies. Z.C., A.M., M.T.F. contributed image analysis and quantification strategies. S.N. contributed electron microscopy. I.D.J., B.H., O.H., A.S.M. contributed design and supervision of experiments. B.H., A.S.M. designed the study. A.S.M. wrote the manuscript. I.D.J., B.H., O.H., A.S.M. contributed funding acquisition. All authors read and approved the manuscript.

Conflicts of interest

M.R. and A.S.M. hold equity in Dynamic42 GmbH. M.R. is CEO of Dynamic42 GmbH. A.S.M. consults to the company.

Data availability

The raw/processed data required to reproduce these findings cannot be shared at this time due to technical or time limitations.

Acknowledgement

We thank Melanie Ulrich, Nora Mosig and Tobias Voigt for excellent technical support. We thank André Scherag for advice on statistical tests. This work was financially supported by the Deutsche Forschungsgemeinschaft (DFG) through the CRC/TR124 FungiNet to I.D.J. (project C5), M.T.F. (project B4) and B.H. (project C1), through the CRC 1278 PolyTarget to M.T.F. (project Z01) and through Cluster of Excellence “Balance of the Microverse”, funded by the Deutsche Forschungsgemeinschaft (DFG, German Research Foundation) under Germany's Excellence Strategy – EXC 2051 – Project-ID 390713860 to I.D.J, M.T.F., B.H. and A.S.M. The work was further financially supported by the German Ministry for Education and Research (BMBF) (grant no. 01EO1002) to I.D.J, O.H., B.H. and A.S.M., an Alexander von Humboldt postdoctoral research fellowship to M.S.G, and though the European Commission through Marie Skłodowska-Curie Actions (MSCA) Innovative Training Network EUROoC (grant no. 812954) to A.S.M.

Appendix A. Supplementary data

Supplementary data to this article can be found online at https://doi.org/10.1016/j.biomaterials.2019.119396.

References

[1] M. Knip, H. Siljander, The role of the intestinal microbiota in type 1 diabetes mellitus, Nat Rev Endocrinol 12 (2016) 154–167, https://doi.org/10.1038/nrendo.2015.218.

[2] L. Zhao, The gut microbiota and obesity: from correlation to causality, Nat Rev Microbiol 11 (2013) 639–647, https://doi.org/10.1038/nrmicro3089.

[3] X.C. Morgan, et al., Dysfunction of the intestinal microbiome in inflammatory bowel disease and treatment, Genome Biol 13 (2012) R79, https://doi.org/10.1186/gb-2012-13-9-r79.

[4] M. Valles-Colomer, et al., The neuroactive potential of the human gut microbiota in quality of life and depression, Nat Microbiol (2019), https://doi.org/10.1038/s41564-018-0337-x.

[5] I.D. Iliev, I. Leonardi, Fungal dysbiosis: immunity and interactions at mucosal barriers, Nat Rev Immunol 17 (2017) 635–646, https://doi.org/10.1038/nri.2017.55.

[6] T.L. Nguyen, S. Vieira-Silva, A. Liston, J. Raes, How informative is the mouse for human gut microbiota research? Dis Model Mech 8 (2015) 1–16, https://doi.org/10.1242/dmm.017400.

[7] J.L. Round, S.K. Mazmanian, The gut microbiota shapes intestinal immune responses during health and disease, Nat Rev Immunol 9 (2009) 313–323, https://doi.org/10.1038/nri2515.

[8] I. Mukhopadhya, R. Hansen, E.M. El-Omar, G.L. Hold, IBD-what role do Proteobacteria play? Nat Rev Gastroenterol Hepatol 9 (2012) 219–230, https://doi.org/10.1038/nrgastro.2012.14.

[9] T. Sato, H. Clevers, Growing self-organizing mini-guts from a single intestinal stem cell: mechanism and applications, Science 340 (2013) 1190–1194, https://doi.org/10.1126/science.1234852.

[10] H.J. Kim, D. Huh, G. Hamilton, D.E. Ingber, Human gut-on-a-chip inhabited by microbial flora that experiences intestinal peristalsis-like motions and flow, Lab Chip 12 (2012) 2165–2174, https://doi.org/10.1039/c2lc40074j.

[11] H.J. Kim, D.E. Ingber, Gut-on-a-Chip microenvironment induces human intestinal cells to undergo villus differentiation, Integr Biol (Camb) 5 (2013) 1130–1140, https://doi.org/10.1039/c3ib40126j.

[12] B.M. Janelsins, M. Lu, S.K. Datta, Altered inactivation of commensal LPS due to acyloxyacyl hydrolase deficiency in colonic dendritic cells impairs mucosal Th17 immunity, Proc Natl Acad Sci U S A 111 (2014) 373–378, https://doi.org/10.1073/pnas.1311987111.

[13] U. Jaffer, R.G. Wade, T. Gourlay, Cytokines in the systemic inflammatory response syndrome: a review, HSR Proc Intensive Care Cardiovasc Anesth 2 (2010) 161–175.

[14] R.L. Chelvarajan, S.M. Collins, J.M. Van Willigen, S. Bondada, The unresponsiveness of aged mice to polysaccharide antigens is a result of a defect in macrophage function, J Leukoc Biol 77 (2005) 503–512, https://doi.org/10.1189/jlb.0804449.

[15] C.C. Bain, A.M. Mowat, Intestinal macrophages - specialised adaptation to a unique environment, Eur J Immunol 41 (2011) 2494–2498, https://doi.org/10.1002/eji.201141714.

[16] D.A. Hume, V.H. Perry, S. Gordon, The mononuclear phagocyte system of the mouse defined by immunohistochemical localisation of antigen F4/80: macrophages associated with epithelia, Anat Rec 210 (1984) 503–512, https://doi.org/10.1002/ar.1092100311.

[17] V. Rossini, et al., CX3CR1(+) cells facilitate the activation of CD4 T cells in the colonic lamina propria during antigen-driven colitis, Mucosal Immunol 7 (2014) 533–548, https://doi.org/10.1038/mi.2013.70.

[18] K.M. Schneider, et al., CX3CR1 is a gatekeeper for intestinal barrier integrity in mice: limiting steatohepatitis by maintaining intestinal homeostasis, Hepatology 62 (2015) 1405–1416, https://doi.org/10.1002/hep.27982.

[19] M. Kim, et al., Critical role for the microbiota in CX3CR1(+) intestinal mononuclear phagocyte regulation of intestinal T cell responses, Immunity 49 (2018) 151–163, https://doi.org/10.1016/j.immuni.2018.05.009 e155.

[20] S. Milling, U. Yrlid, V. Cerovic, G. MacPherson, Subsets of migrating intestinal dendritic cells, Immunol Rev 234 (2010) 259–267, https://doi.org/10.1111/j.0105-2896.2009.00866.x.

[21] J. Farache, et al., Luminal bacteria recruit CD103+ dendritic cells into the intestinal epithelium to sample bacterial antigens for presentation, Immunity 38 (2013) 581–595, https://doi.org/10.1016/j.immuni.2013.01.009.

[22] T. Worbs, et al., Oral tolerance originates in the intestinal immune system and relies on antigen carriage by dendritic cells, J Exp Med 203 (2006) 519–527, https://doi.org/10.1084/jem.20052016.

[23] M. Raasch, et al., Microfluidically supported biochip design for culture of endothelial cell layers with improved perfusion conditions, Biofabrication 7 (2015) 015013, , https://doi.org/10.1088/1758-5090/7/1/015013.

[24] H. Zalzali, et al., CEACAM1, a SOX9 direct transcriptional target identified in the colon epithelium, Oncogene 27 (2008) 7131–7138, https://doi.org/10.1038/onc.2008.331.

[25] S.W. Craig, L.D. Powell, Regulation of actin polymerization by villin, a 95,000 dalton cytoskeletal component of intestinal brush borders, Cell 22 (1980) 739–746.

[26] R. Noth, et al., Increased intestinal permeability and tight junction disruption by altered expression and localization of occludin in a murine graft versus host disease model, BMC Gastroenterol 11 (2011) 109, https://doi.org/10.1186/1471-230X-11-109.

[27] J. Sun, et al., Crosstalk between NF-kappaB and beta-catenin pathways in bacterial-colonized intestinal epithelial cells, Am J Physiol Gastrointest Liver Physiol 289 (2005) G129–G137, https://doi.org/10.1152/ajpgi.00515.2004.

[28] G. Luo, T. Guenthner, L.S. Gan, W.G. Humphreys, CYP3A4 induction by xenobiotics: biochemistry, experimental methods and impact on drug discovery and development, Curr Drug Metab 5 (2004) 483–505.

[29] O. Medina-Contreras, et al., CX3CR1 regulates intestinal macrophage homeostasis, bacterial translocation, and colitogenic Th17 responses in mice, J Clin Invest 121 (2011) 4787–4795, https://doi.org/10.1172/JCI59150.

[30] A.R. Tanner, M.J. Arthur, R. Wright, Macrophage activation, chronic inflammation and gastrointestinal disease, Gut 25 (1984) 760–783.

[31] F. Sanchez-Munoz, A. Dominguez-Lopez, J.K. Yamamoto-Furusho, Role of cytokines in inflammatory bowel disease, World J Gastroenterol 14 (2008) 4280–4288.

[32] A. Kaser, S. Zeissig, R.S. Blumberg, Inflammatory bowel disease, Annu Rev Immunol 28 (2010) 573–621, https://doi.org/10.1146/annurev-immunol-030409-101225.

[33] W.E. Cromer, J.M. Mathis, D.N. Granger, G.V. Chaitanya, J.S. Alexander, Role of the endothelium in inflammatory bowel diseases, World J Gastroenterol 17 (2011) 578–593, https://doi.org/10.3748/wjg.v17.i5.578.

[34] J. Zhang, A.F. Defelice, J.P. Hanig, T. Colatsky, Biomarkers of endothelial cell activation serve as potential surrogate markers for drug-induced vascular injury, Toxicol Pathol 38 (2010) 856–871, https://doi.org/10.1177/0192623310378866.

[35] A.L. Hart, et al., Homing of immune cells: role in homeostasis and intestinal inflammation, Inflamm Bowel Dis 16 (2010) 1969–1977, https://doi.org/10.1002/ibd.21304.

[36] L. Laval, et al., Lactobacillus rhamnosus CNCM I-3690 and the commensal bacterium Faecalibacterium prausnitzii A2-165 exhibit similar protective effects to induced barrier hyper-permeability in mice, Gut Microbes 6 (2015) 1–9, https://doi.org/10.4161/19490976.2014.990784.

[37] M.I. Alvarez-Olmos, R.A. Oberhelman, Probiotic agents and infectious diseases: a modern perspective on a traditional therapy, Clin Infect Dis 32 (2001) 1567–1576, https://doi.org/10.1086/320518.

[38] V.H. Matsubara, H.M. Bandara, M.P. Mayer, L.P. Samaranayake, Probiotics as antifungals in mucosal candidiasis, Clin Infect Dis 62 (2016) 1143–1153, https://doi.org/10.1093/cid/ciw038.

[39] T.M. Forster, et al., Enemies and brothers in arms: Candida albicans and gram-positive bacteria, Cell Microbiol 18 (2016) 1709–1715, https://doi.org/10.1111/cmi.12657.

[40] M.E. Bougnoux, et al., Multilocus sequence typing reveals intrafamilial transmission and microevolutions of Candida albicans isolates from the human digestive tract, J Clin Microbiol 44 (2006) 1810–1820, https://doi.org/10.1128/JCM.44.5.1810-1820.2006.

[41] A. Zaborin, et al., Membership and behavior of ultra-low-diversity pathogen communities present in the gut of humans during prolonged critical illness, MBio 5 (2014) 01314, https://doi.org/10.1128/mBio.01361-14 e01361.

[42] K.M. James, K.W. MacDonald, R.M. Chanyi, P.A. Cadieux, J.P. Burton, Inhibition of Candida albicans biofilm formation and modulation of gene expression by probiotic cells and supernatant, J Med Microbiol 65 (2016) 328–336, https://doi.org/10.1099/jmm.0.000226.

[43] G.A. Kohler, S. Assefa, G. Reid, Probiotic interference of Lactobacillus rhamnosus GR-1 and Lactobacillus reuteri RC-14 with the opportunistic fungal pathogen Candida albicans, Infect Dis Obstet Gynecol (2012) 636474, https://doi.org/10.1155/2012/636474 2012.

[44] M. Strus, et al., The in vitro activity of vaginal Lactobacillus with probiotic properties against Candida, Infect Dis Obstet Gynecol 13 (2005) 69–75, https://doi.org/10.1080/10647440400028136.

[45] A. Rizzo, A. Losacco, C.R. Carratelli, Lactobacillus crispatus modulates epithelial cell defense against Candida albicans through Toll-like receptors 2 and 4, interleukin 8 and human beta-defensins 2 and 3, Immunol Lett 156 (2013) 102–109, https://doi.org/10.1016/j.imlet.2013.08.013.

[46] D. Mailander-Sanchez, et al., Antifungal defense of probiotic Lactobacillus rhamnosus GG is mediated by blocking adhesion and nutrient depletion, PLoS One 12 (2017) e0184438, , https://doi.org/10.1371/journal.pone.0184438.

[47] M.S. do Carmo, et al., Lactobacillus fermentum ATCC 23271 displays in vitro inhibitory activities against Candida spp, Front Microbiol 7 (2016) 1722, https://doi.org/10.3389/fmicb.2016.01722.

[48] M.D. Peterson, M.S. Mooseker, Characterization of the enterocyte-like brush border cytoskeleton of the C2BBe clones of the human intestinal cell line, Caco-2, J Cell Sci 102 (Pt 3) (1992) 581–600.

[49] B.J. van Klinken, et al., The human intestinal cell lines Caco-2 and LS174T as models to study cell-type specific mucin expression, Glycoconj J 13 (1996) 757–768.

[50] H.J. Kim, H. Li, J.J. Collins, D.E. Ingber, Contributions of microbiome and mechanical deformation to intestinal bacterial overgrowth and inflammation in a human gut-on-a-chip, Proc Natl Acad Sci U S A 113 (2016) E7–E15, https://doi.org/10.1073/pnas.1522193112.

[51] P. Shah, et al., A microfluidics-based in vitro model of the gastrointestinal human-microbe interface, Nat Commun 7 (2016) 11535, https://doi.org/10.1038/ncomms11535.

[52] C.C. Bain, et al., Constant replenishment from circulating monocytes maintains the macrophage pool in the intestine of adult mice, Nat Immunol 15 (2014) 929–937, https://doi.org/10.1038/ni.2967.

[53] I. Amit, D.R. Winter, S. Jung, The role of the local environment and epigenetics in shaping macrophage identity and their effect on tissue homeostasis, Nat Immunol 17 (2016) 18–25, https://doi.org/10.1038/ni.3325.

[54] F. Ginhoux, M. Guilliams, Tissue-resident macrophage ontogeny and homeostasis, Immunity 44 (2016) 439–449, https://doi.org/10.1016/j.immuni.2016.02.024.
[55] C.C. Bain, et al., Resident and pro-inflammatory macrophages in the colon represent alternative context-dependent fates of the same Ly6Chi monocyte precursors, Mucosal Immunol 6 (2013) 498–510, https://doi.org/10.1038/mi.2012.89.
[56] P. Krause, et al., IL-10-producing intestinal macrophages prevent excessive antibacterial innate immunity by limiting IL-23 synthesis, Nat Commun 6 (2015) 7055, https://doi.org/10.1038/ncomms8055.
[57] I. Leonardi, et al., CX3CR1(+) mononuclear phagocytes control immunity to intestinal fungi, Science 359 (2018) 232–236, https://doi.org/10.1126/science.aao1503.
[58] L.E. Smythies, et al., Human intestinal macrophages display profound inflammatory anergy despite avid phagocytic and bacteriocidal activity, J Clin Invest 115 (2005) 66–75, https://doi.org/10.1172/JCI19229.
[59] J. Cosin-Roger, et al., The activation of Wnt signaling by a STAT6-dependent macrophage phenotype promotes mucosal repair in murine IBD, Mucosal Immunol 9 (2016) 986–998, https://doi.org/10.1038/mi.2015.123.
[60] J.E. Qualls, A.M. Kaplan, N. van Rooijen, D.A. Cohen, Suppression of experimental colitis by intestinal mononuclear phagocytes, J Leukoc Biol 80 (2006) 802–815, https://doi.org/10.1189/jlb.1205734.
[61] T.L. Denning, et al., Functional specializations of intestinal dendritic cell and macrophage subsets that control Th17 and regulatory T cell responses are dependent on the T cell/APC ratio, source of mouse strain, and regional localization, J Immunol 187 (2011) 733–747, https://doi.org/10.4049/jimmunol.1002701.
[62] C.L. Scott, et al., Bone marrow-derived monocytes give rise to self-renewing and fully differentiated Kupffer cells, Nat Commun 7 (2016) 10321, https://doi.org/10.1038/ncomms10321.
[63] M. Groger, et al., Monocyte-induced recovery of inflammation-associated hepatocellular dysfunction in a biochip-based human liver model, Sci Rep 6 (2016) 21868, https://doi.org/10.1038/srep21868.
[64] H.Y. Liu, et al., Effects of Lactobacillus johnsonii and Lactobacillus reuteri on gut barrier function and heat shock proteins in intestinal porcine epithelial cells, Physiol Rep 3 (2015), https://doi.org/10.14814/phy2.12355.
[65] G. Bamias, D.J. Clark, J. Rivera-Nieves, Leukocyte traffic blockade as a therapeutic strategy in inflammatory bowel disease, Curr Drug Targets 14 (2013) 1490–1500.
[66] S. Mosig, et al., Different functions of monocyte subsets in familial hypercholesterolemia: potential function of CD14+ CD16+ monocytes in detoxification of oxidized LDL, FASEB J 23 (2009) 866–874, https://doi.org/10.1096/fj.08-118240.